CrystEngComm

Supramolecular open-framework architectures based on dicarboxylate H-bond acceptors and polytopic cations with three/four N-H+ donor units

Journal:	*CrystEngComm*
Manuscript ID:	CE-ART-06-2015-001070.R3
Article Type:	Paper
Date Submitted by the Author:	09-Jul-2015
Complete List of Authors:	Mouchaham, Georges; Laboratoire de Chimie de Coordination du CNRS, Gualino, Marion; Laboratoire de Chimie de Coordination du CNRS, Roques, Nans; CNRS, Laboratory of Coordination Chemistry Duhayon, Carine; Laboratoire de Chimie de Coordination du CNRS, Brandès, Stéphane; Universite de Bourgogne, Sutter, Jean-Pascal; Laboratoire de Chimie de Coordination du CNRS,

Supramolecular open-framework architectures based on dicarboxylate H-bond acceptors and polytopic cations with three/four N-H$^+$ donor units.

Georges Mouchaham,[a,b] Marion Gualino,[a,b] Nans Roques,*[a,b] Carine Duhayon, [a,b] Stéphane Brandès[c] and Jean-Pascal Sutter *[a,b]

[a] CNRS, LCC (Laboratoire de Chimie de Coordination), 205 route de Narbonne, F-31077 Toulouse, France. E-mail: nans.roques@lcc-toulouse.fr, sutter@lcc-toulouse.fr

[b] Université de Toulouse, UPS, INPT, LCC, F-31077, Toulouse, France.

[c] ICMUB (Institut de Chimie Moléculaire de l'Université de Bourgogne), UMR 6302 CNRS, Université de Bourgogne, F-21078, Dijon, France.

Graphical abstract

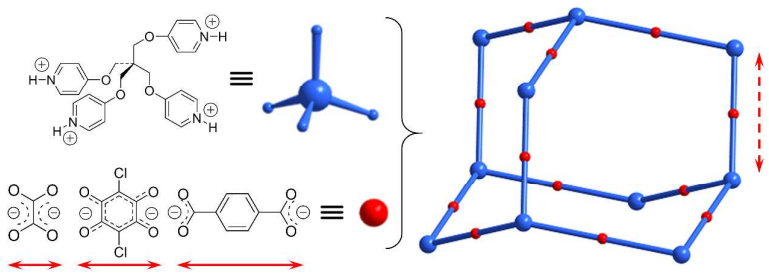

Abstract:

Supramolecular assemblages based on anionic H-acceptors and cationic H-donors have been envisioned to elaborate open frameworks maintained by ionic H-bonds. Combinations of di-anionic chloranilate (CA^{2-}), oxalate (Ox^{2-}), or terephtalate (BDC^{2-}) and trisimidazolium or tetrapyridinium derivatives (respectively three and four N-H^{+} donors), yielded five architectures of formula $[\{(H_3TrIB)(CA)_{1.5}\}\cdot 2DMF\cdot 2.5H_2O]$ (**1**), $[\{(H_4Tetrapy)(CA)_2\}\cdot 3DMF]$ (**2**), $[\{(H_3TrIB)(HOx)(Ox)\}\cdot 5H_2O]$ (**3**), $[\{(H_4Tetrapy)(Ox)_2\}\cdot 5H_2O]$ (**4**), and $[\{(H_4Tetrapy)(BDC)_2(H_2O)\}\cdot 1DMF\cdot 3H_2O]$ (**5**) (with TrIB = 1,3,5-trisimidazolylbenzene and Tetrapy = tetrakis[(pyridine-4-yloxy)methyl]methane). Four of these, *i.e.* **1**, **2**, **4** and **5**, show an open framework. Their assembling patterns and framework dimensionalities are mainly governed by the chemical features of the cation. 1D (**3**) and 2D (**1**) networks are found with $[H_3TrIB]^{3+}$ whereas 3D diamond-type netwoks (**2**, **4**, **5**) are systematically formed with $[H_4Tetrapy]^{4+}$. While the individual adamantanoid cages exhibit large voids in all 3D structures, net catenations (with a total degree of interpenetration up to 19) reduce the potential porosities of the solids to 17-32%. The largest solvent accessible void (42%) is found for the 2D supramolecular organization of **1**, for which net interpenetration does not take place. Crystal structures for all five architectures are reported. Framework robustness upon guest departure and gas sorption properties has been explored for materials **1** and **2** with the highest potential accessible voids.

Introduction

Hydrogen-bonded (H-bonded) multicomponent crystalline materials comprised of neutral or charged organic molecules (co-crystals[1] and ionic salts,[2] respectively) are highly studied compounds in the field of crystal engineering,[3] both for their pharmaceutical importance[4] and their solid state architectures.[5] In this latter area, an important topic concerns the synthesis of supramolecular materials with a specific geometric or topological structure to achieve a given chemical or physical property.[6] This implies to gain control over the formation of the structure corresponding to the targeted property, in order to subsequently optimize the material's performance by chemical design.

Recent reports have demonstrated the potential of purely organic H-bonded architectures as porous materials.[7] However, while the combination of carboxylic acid and pyridyl groups has been widely used to form H-bonded co-crystals via COOH···N(Py) linkage, [7f, 8] permanent porosity and high CO_2 sorption have been evidenced only very recently for one of them.[7f] Reason for this lack of success is found in the framework/crystal structure flexibility (leading to a collapse of the cavities on removal of the guests)[9] and/or interpenetration,[8e, 10] which are commonplaces for many molecular materials. Moreover, the possibility to prevent or restrict these issues by chemical means appears challenging in co-crystals.

The solid state structure of the molecular material is reliant on patterns of supramolecular interactions working between the molecular components (i.e. the supramolecular synthons).[6b, 11] In assemblages involving components having two different functionalities such as carboxylic acid and pyridyl moieties, competition between the desired hetero-synthons and homo-synthons (carboxylic acids can auto-assemble by means of H-bonds) is often observed.[8b-d] Moreover, the solvent used in the crystallization process could also play a role by interfering with the anticipated assembling pattern.[12] Finally and not least, a small alteration of a molecular unit frequently induces changes in a native supramolecular synthon,[2b, 8c, 8f] and by extension important modifications for the resulting structure. Therefore, tuning the functionality of a given supramolecular framework often turns impossible.

A way to circumvent the versatility of the molecular assemblage is to involve a supramolecular interaction strong enough to override the other weaker intermolecular forces taking place in the crystal packing. Such a prevailing interaction is expected to dictate the

basic assembling scheme, hence making predictable the synthon formation despite alteration of the building-blocks. It should also impede homo-synthon formation, and it could further contribute improving the framework robustness upon guest (solvent) release from the solid material. Such a stronger supramolecular synthon is provided by charge-assisted or ionic H-bonds, which bond strengths of 20-140 $kJ.mol^{-1}$ position them in the upper part of the energy scale of hydrogen bonds.[13] This approach has been illustrated by the pioneering work of Ward et *al.*,[14] who have investigated the systematic formation and structural features of a variety of open-framework architectures based on guanidine and disulfonic acids ($R(SO_3H)_2$). In these structures, two dimensional hydrogen-bonded sheets comprising guanidinium and sulfonates are interconnected by R pillars to yield grid-like architectures with one-dimensional pores. Pore properties were easily modulated by adapting the R group characteristics. More recently, Tohnai *et al.* have combined predictable ionic H-bonds and weaker interactions (such π···π interactions[15] or classical H-bonds[16]) to form and subsequently assemble supramolecular building units in modular diamond frameworks. We have reported several examples of open-framework and porous architectures maintained by ionic H-bonds made of negatively charged metallo-tectons (typically metal-oxalate complexes acting as H-bond acceptors) and organic cations (the H-bond donors).[17] Herein, we extended this approach for the tentative elaboration of purely organic open-framework materials.

Two cationic H-bond donors, H_3TrIB^{3+} (TrIB = 1,3,5-trisimidazolylbenzene) and the $H_4Tetrapy^{4+}$ (Tetrapy = tetrakis[(pyridine-4-yloxy)methyl]methane), have been selected for their geometrical characteristics and their charges. They are anticipated to act as T-shaped 3-connecting and tetrahedral-shaped 4-connecting H-bond donors, respectively (See scheme 1, top). These have been associated to di-anionic 2-connecting H-bond acceptors, *i.e.* chloranilate (CA^{2-}), oxalate (Ox^{2-}), or terephtalate (BDC^{2-}), in order to yield 2D (grid-like) and 3D (diamond-like) networks sustained by ionic H-bonds. For a given network, changing the size of the H-bond acceptor (Scheme 1, bottom) was considered to tune the distances between the nodes and hence the potential porosity of the structure. Four out of the six donor/acceptor combinations yielded open-framework architectures. Three of them involve the tetracation, and show the anticipated diamond-like H-bonded organisation. Despite network interpenetration (from 6- to 19-fold) these structures exhibit solvent accessible void. Framework robustness upon guest departure, and gas sorption properties have been explored for the two materials with largest potential porosities.

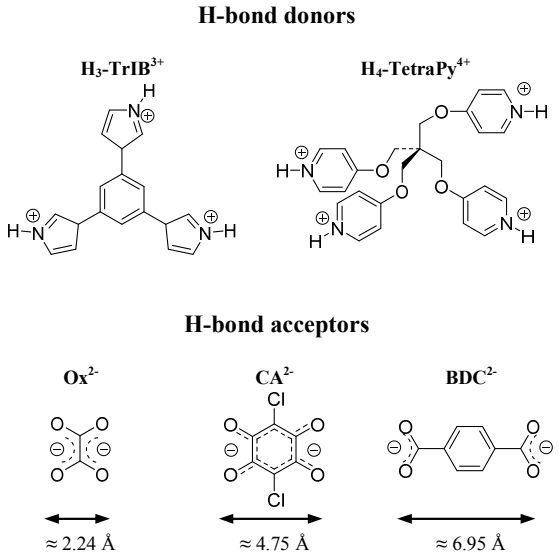

Scheme 1.

Results and discussion

Synthesis

Networks **1-5** were obtained in DMF/H_2O 95/5 mixture (DMF stands for N,N-dimethyl formamide), by reacting TrIB[18] and Tetrapy[19] with charge-stoichiometry amounts (1.5 and 2 eq., respectively) of the diacids H_2Ox, H_2CA, and H_2BDC. For the sake of comparison, the molarity in amine derivative was same in each case. Proton transfer from acidic to basic sites occurs when reagents are mixed yielding the actual building-blocks listed in Scheme 1. With H_2CA, proton transfer is clearly visible by a colour change of the solutions from red to dark violet. Charge stoichiometry compounds of formula $[\{(H_3TrIB)(CA)_{1.5}\}\cdot 2DMF\cdot 2.5H_2O]$ (**1**), $[\{(H_4Tetrapy)(CA)_2\}\cdot 3DMF]$ (**2**), $[\{(H_3TrIB)(H\text{-}Ox)(Ox)\}\cdot 5H_2O]$ (**3**), $[\{(H_4Tetrapy)(Ox)_2\}\cdot 5H_2O]$ (**4**), and $[\{(H_4Tetrapy)(BDC)_2(H_2O)\}\cdot 1DMF\cdot 3H_2O]$ (**5**) were crystallized in good yields (38-80%) from these mixtures. For associations involving H_2CA, microcrystalline powders form immediately upon mixing the reagents. Single crystals of **1** and **2** suitable for XRD studies have been obtained through recrystallization. With H_2Ox and H_2BDC, single crystals of **3**, **4** and **5** were formed by keeping undisturbed reagent mixtures over 48h. In these conditions, assemblages between H_3-$TrIB^{3+}$ and BDC^{2-} systematically yielded microcrystalline powders; growing good quality single crystals remained unsuccessful with these building-blocks even by changing the crystallization conditions and reagents' ratios. The crystal structures have been solved for compounds **1-5**, and their chemical

composition was confirmed by thermogravimetric analysis and elemental analysis (see Experimental Section and ESI).

Crystal structures

Crystal structures for **1-5** have been determined by single crystal X-ray diffraction (SCXRD), crystallographic data and structure-refinement parameters are listed in Table S1 (ESI). Plots of the asymmetric units showing thermal ellipsoids and atom labelling are provided in ESI, as well as H-bond lengths and angles (Table S2). H atoms have been positioned in theoretical positions, except for **3** where they have been located in a Fourrier difference map. From the comparison between observed C–O bond distances in the CA^{2-} units of structures **1** and **2** (1.232 Å to 1.260 Å) and the bond lengths found in H_2CA (1.225 Å and 1.320 Å),[20] it can be concluded that the two supramolecular architectures **1** and **2** are molecular salts rather than co-crystals. Related reasoning for the structures involving Ox^{2-} and BDC^{2-} spacers lead to the same conclusion. For this reason, acidic hydrogen atoms have been systematically placed on N atoms when their position could not be deduced from SCXRD data.

$[\{(H_3TrIB)(CA)_{1.5}\}\cdot 2DMF\cdot 2.5H_2O]$, **1**, crystallizes in the monoclinic space group $P2_1/c$, with one H_3TrIB^{3+}, one and a half CA^{2-}, two DMF (one and two halves) and two and a half H_2O molecules packed in the asymmetric unit (Fig. S1 in ESI).[21] It might be noticed that in H_3TrIB two of the imidazolium rings lie almost coplanar with the benzene core whereas the third ring is slightly out-of-plane with a dihedral angle of 20.5°. On a supramolecular point of view, each H_3TrIB^{3+} is linked to three CA^{2-} anions by means of H-bonds established between an imidazolium $N\text{-}H^+$ group and two oxygen atoms of an acceptor unit (Fig. S2), and each CA^{2-} is connected with two imidazolium moieties from different $H_3\text{-}TrIB^{3+}$ (Fig. 1). Since the three $N\text{-}H^+$ groups of the donor unit are almost coplanar, this association scheme results in neutral 2D H-bonded networks developing in the *ab* plan. These can be described as grids formed by interconnected $[H_3TrIB\text{-}CA]_6$ rhomboidal windows of *ca* 25.3 × 6.4 $Å^2$ in dimension. Additional close Cl···Cl contacts between CA units (two per windows) reinforce these H-bonded associations.[22] Assimilating H_3TrIB^{3+} cations to nodes and CA^{2-} anions to linkers, the topology of this H-bonded architecture is described as a 6^3 net by the Schläfli symbol.[23] Examination of the structure along the *c*-axis reveals an ABAB-type packing of the layers. This packing involves π···π interactions between H_3TrIB^{3+} and CA^{2-} units belonging to consecutive layers (Fig. S3 and S4). It generates large oval 1D channels (~ 6 × 9 Å) running along the *a*-axis, and smaller pores (~ 6 × 3 $Å^2$) along [101] crystallographic direction (Fig. 1c and S5). Based on PLATON calculations,[24] these channels endow this material with a solvent

accessible void volume of 41%. In absolute terms, it represents a volume of 1536.8 $Å^3$ per 3712.7 $Å^3$ of the unit cell. This space is occupied by DMF and H_2O molecules.

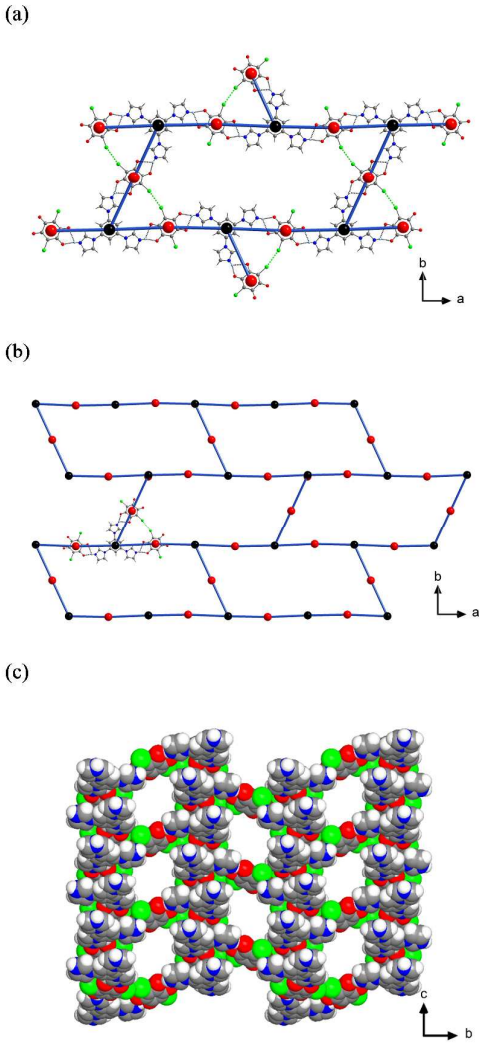

Fig. 1. Supramolecular architecture of **1**. (a) 12-membered supramolecular window. (b) Topological representation of a 2D H-bonded grid in **1** . (c) Space-filling representation of **1** showing 1D channels. Color codes in (a) and (c): C, grey; H, white; N, blue; Cl, green and O, red.

[{(H_4Tetrapy)($CA)_2$}·3DMF], **2**, crystallizes in the monoclinic space group $P2_1/c$, with one $H_4Tetrapy^{4+}$, two CA^{2-} (*i.e.*, one and two halves which lie about independent inversion centres) and three DMF molecules packed in the asymmetric unit (see Fig. S6 in ESI). Hydrogen bonding takes place between the pyridinium N-H^+ groups and the CA^{2-} units. Each $H_4TetraPy^{4+}$ interacts with four CA^{2-} and each H-bond acceptor unit links two $H_4Tetrapy^{4+}$ cations. (Fig. S7, ESI). In $H_4Tetrapy^{4+}$, the pyridinium groups are directed in the three directions of space, as a result the ionic hydrogen bond association leads to 3D diamondoid

(**dia**) net.[10] A view of an adamantanoid cage of this network is given in Fig. 2a. The cage metrics slightly differ from the ones expected for a perfect adamantanoid cage,[8c] with edges values of 21.76 and 21.90 Å, which correspond to the distances between central C atoms of H_4Tetrapy^{4+}nodes. The overall structure of **2** consists of interpenetrating diamondoid nets with a total degree of interpenetration of 7. Each individual net is translated along the *a*-axis (Fig 2b).[10] Despite this 7-fold catenation, the structure contains solvent molecules (DMF and H_2O, see table S3) located in channel running along *a*-axis. These channels exhibit an aperture of ~ 6.5 × 2.5 Å^2 (after taking into account the van der Walls radii of the surrounding atoms) and endow the solid with a solvent accessible void volume of 32%.[24]

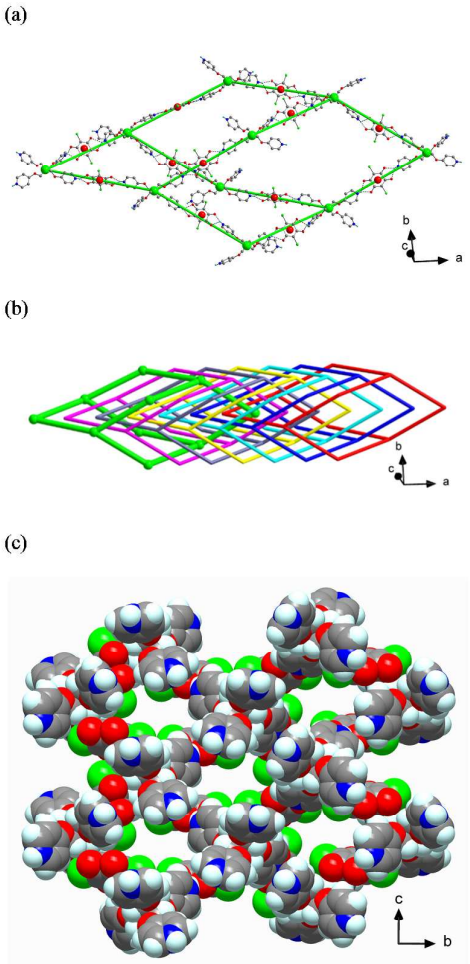

Fig. 2. Supramolecular architecture of **2**. (a) Single adamantanoid cage (b) Schematic view of the 7-fold interpenetration. (c) Space-filling representation of the complete structure (comprising all nets) of **2**, showing the channels running along *a* (guest molecules are omitted for clarity). Colour codes in (a) and (c): C, grey; H, white; N, blue; Cl, green and O, red. In (b), each colour designates an independent adamantanoid cage.

[{(H_3TrIB)(HOx)(Ox)}·5H_2O], **3**, crystallizes in the monoclinic space group $P2_1/c$ and consists in a neutral architecture based on corrugated H-bonded tapes. They result from the assemblage between H_3TriB^{3+} and oxalate dimers involving partially and fully deprotonated HOx^-/Ox^{2-} units (Fig. 3 and S8, ESI). π···π interactions lead to the packing of these tapes along the *c* crystallographic direction. The resulting supramolecular walls sandwich water molecules, which are H-bonded with oxalates and H_3TriB^{3+} belonging to walls (Fig. S9).

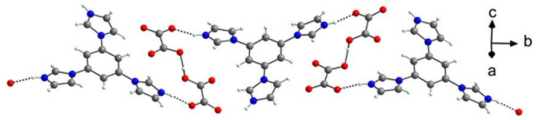

Fig. 3. H-bonded supramolecular tape in the structure of $\mathbf{3_{Ox}}$, [{(H_3TrIB)(HOx)(Ox)}·5H_2O]. Color codes: C, grey; H, white; N, blue and O, red. The asymmetric unit is shown in Fig. S8; packing is illustrated in Fig. S9 (EDI).

[{(H_4Tetrapy)($Ox)_2$}·5H_2O], **4**, crystallizes in the tetragonal space group $I4_1/a$, with two and a half $H_4Tetrapy^{4+}$ and five Ox^{2-} packed in the asymmetric unit (Fig. S10). The half $H_4Tetrapy^{4+}$ lies with C87 on a twofold axis. The supramolecular synthons observed in **4** are identical to the ones found in **2** (details are given in Fig. S11), and the resulting H-bonded assemblage also corresponds to a 3D diamandoid net. However, the metrics of the adamantanoid cages of **4** are reduced (Table 1) in agreement with the smaller oxalate linker. The overall structure consists of interpenetrating nets with a total degree of interpenetration of 6. Two sets of crystallographically distinct nets (A and B, Fig. 4a) occur in the framework of **4**; these nets alternate and translate along *c*-axis (Fig. 4b). Narrow 1D pores, showing a square section of 2.5 Å in diagonal (van der Waals radii are deducted), are observed along *c*-axis (Fig 4c); they contain H_2O molecules. These were found to be highly disordered but the number of electrons associated to the guests allowed to estimate a composition of 5 H_2O per formula unit (see experimental section). This composition has been ascertained by TGA and elemental analysis (Table S3, ESI). When these guest molecules are neglected, a solvent accessible volume of 17% is calculated using PLATON.[24]

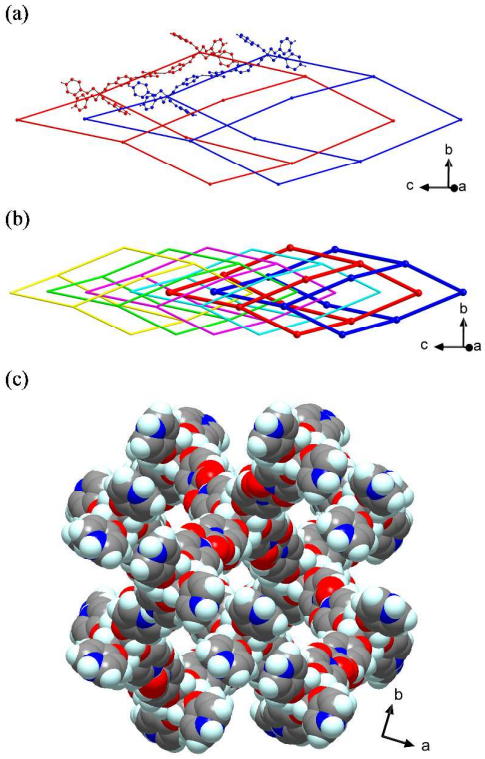

Fig. 4. Supramolecular architecture of **4**. (a) Two crystallographically distinct H-bonded nets, A (blue) and B (red, supramolecular synthons are detailed in Fig. S11). (b) Schematic view of the 6-fold interpenetration (A cages are represented in blue, light blue and green; B cages in red, pink and yellow). (c) Space-filling representation of **4** showing 1D pores of square section (guest molecules are omitted for clarity). Colour codes in (c): C, grey; H, white; N, blue and O, red.

[{(H_4-Tetrapy)$(BDC)_2(H_2O)$}·1DMF·3H_2O], **5**, crystallizes in the triclinic space group *P*-1, with one H_4-$TetraPy^{4+}$, four halves of BDC^{2-}, 1 DMF and 4 H_2O packed in the asymmetric unit (Fig. S12, ESI). The four halves of BDC^{2-} lie about independent inversion centers. For this system too, a 3D diamond network results from hydrogen bonding between the molecular units. However, one of the H_2O molecules (O63) is involved as supramolecular bridge between carboxylate and pyridinium groups in three of the twelve edges of the adamantanoid cages of this material (see Fig. S13 and S14 for details on H-bonds). Consequently, added to the edge length enlargement expected from the use of the BDC^{2-} spacer (from an average length of 21.85 Å in **2** to 24.76Å in **5**, see Table 1), three out of the twelve edges have their length increased to 30.01 Å by the additional H_2O. Due to the large space available, a 19-fold net interpenetration is observed (Fig. 5). These are organized in five sets of interpenetrated nets shifted by 12.51 Å along *b* direction (Fig. 5b). Four sets comprise 4 nets and the fifth is

composed by 3 nets, all are separated by 10.30 Å along *a*-axis (Fig. 5b). The network interpenetration described above generates an open-framework showing narrow channels (~ 2 × 2 $Å^2$) along the *a* direction (Fig. S15); these channels interconnect pockets where H_2O and DMF molecules are hosted. When these guests are neglected, a solvent accessible volume of 17% is calculated by PLATON.

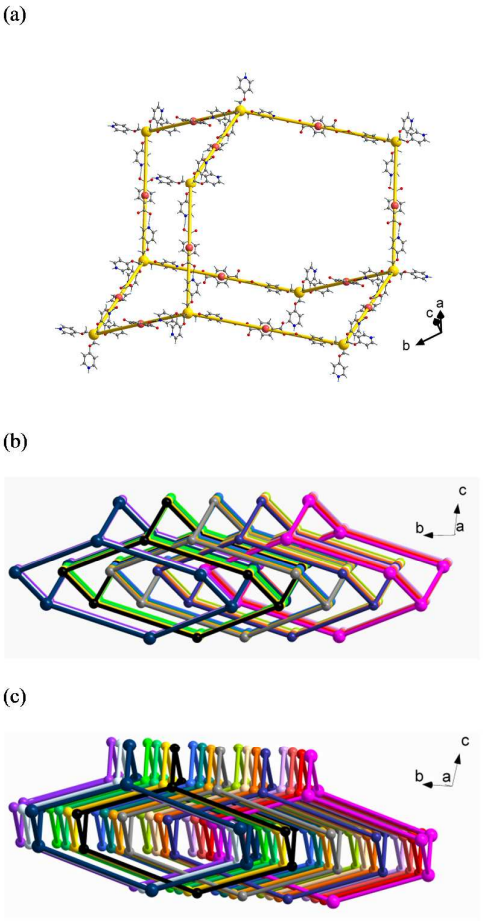

Fig. 5. Supramolecular architecture of **5**. (a) Detail of the H-bonded assemblage for one network (b) schematic view of the five sets of interpenetrated nets shifted by *b*. (b) view showing the 19 interpenetrating nets.

This series of assemblages clearly illustrates the dominant role played by the ionic H-bond in the association of the molecular building-units. Especially the 3D networks formed with the $[Tetrapy]^{4+}$ unit (i.e. **2**, **4**, and **5**), for which the H-bond acceptor could be varied without altering the overall network organization. Considering that Ox, CA and BDC are quite different species this is rather gratifying and confirms the robustness of the supramolecular synthon used herein.

Table 1. Summary of the structural features for diamandoid frameworks **2**, **4**, and **5**.

	2	**4**	**5**
Formula	[{(H_4Tetrapy)($CA)_2$}·3DMF]	[{(H_4Tetrapy)($Ox)_2$}·5H_2O]	[{(H_4Tetrapy)($BDC)_2$(H_2O)}·1DMF·3H_2O]
Edge length in adamantanoid cages	21.76 and 21.90 Å	from 19.17 to 19.28 Å (for A) from 19.19 to 19.39 Å (for B)	from 24.47 to 24.76 Å and 30.01 Å [a]
n-fold interpenetration	7	6	19
Pore aperture	~ 6.5 × 2.5 $Å^2$	~ 2 × 2 $Å^2$	~ 2 × 2 $Å^2$
Solvent accessible void volume[24]	32.0%	17.4%	17.0%

[a] 2 H_2O molecules are involved as supramolecular bridges between BDC carboxylates and pyridinium groups in three out of the twelve edges.

Framework robustness and gas sorption properties for 1 and 2

Compounds **1** and **2,** with the highest potential accessible voids, were subjected to TGA and variable temperature PXRD experiments to evaluate the robustness of their framework upon guests' departure. Comparable behaviours have been observed for the two materials. As soon as they are removed from their mother liquors, the crystalline materials lose part of their guest molecules. TGA (Fig.S16, ESI) indicate a first weight loss upon heating to 120°C which corresponds to complete departure of guests, while chemical decomposition of the frameworks takes place above 200°C.

The PXRD pattern for freshly isolated samples of **1** and **2** is in good agreement with the diffractogram calculated from SCXRD data (Fig. 6 and S17 in ESI). The slight peak displacements and/or intensity variations are ascribed to the temperature at which data collection have been performed (RT for PXRD *versus* cryogenic temperatures for SCXRD) and to preferential orientation effects. This is confirmed by unit cell parameters obtained by Le Bail analysis[25] which reveal minor deformation of the framework for pristine, freshly isolated, materials. Signs for structure deformation and amorphisation are observed after activation under vacuum (6h at 23°C). This is revealed by slights shift and broadening of the peaks, together with peaks intensity decrease. Interestingly, when the activated materials were immersed in DMF for 2h, at RT, the initial phase was recovered for **2** (Fig. 6) while a new phase was found for **1** (Fig. S17). This novel phase is rationalized by the absence of H_2O which is part of the guest molecules in the pristine material **1**. It is worth recalling that materials **1** and **2** are insoluble in DMF and common organic solvents at RT and that they

have been immerged in DMF for a short period of time, therefore a dissolution/re-crystallization process to account for the recovery of the guests can be excluded.

From these PXRD studies it can be concluded that the frameworks of **1** and **2** exhibit some flexibility upon guest release but their integrity is not affected. Moreover, they recover their crystalline by re-sorption of their guests (i.e. DMF), confirming their open-framework features.

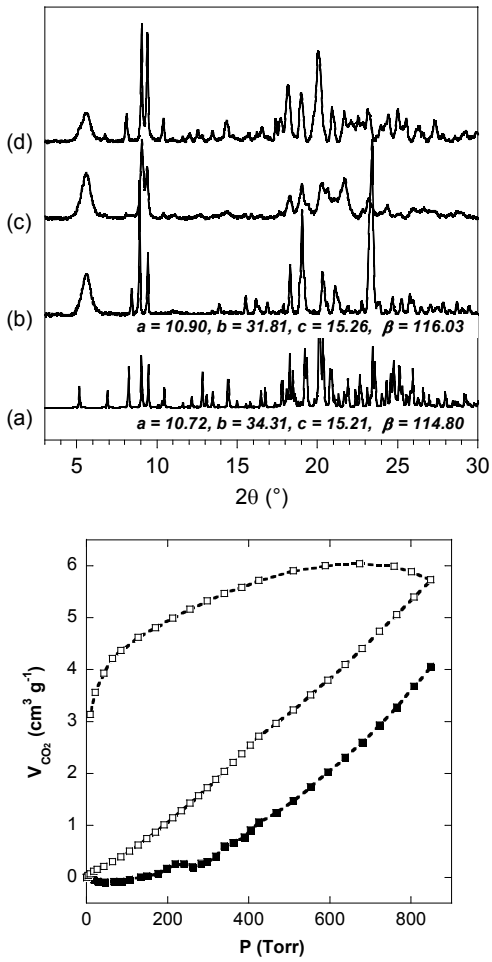

Fig. 6. *(top)* PXRD patterns for **2** (a) calculated from SCXRD data; (b) as-synthesized powder; (c) vacuum activated powder, and (d) after immersion of the activated phase in DMF. Bump/peak enlargement observed in b and c at 2θ = 6° is ascribed to the kapton holder used for measurements. (*bottom)* CO_2 sorption isotherms registered at 25°C for activated **1** (□) and **2** (■).

Gas sorption isotherms have been recorded for activated **1** and **2** with N_2 and CO_2. The poor N_2-adsorption at 77 K revealed absence of permanent porosity likely due to a squeezing of the framework upon guest release. As a consequence, the pore apertures are close after solvent removal. This was confirmed by the CO_2 sorption isotherms obtained at 25°C that shows

moderate but progressive increase of adsorbed volumes of gas with pressure (Fig. 6). Such a profile indicates a progressive opening of the pores as the CO_2 pressure is increased. However, CO_2 uptakes (5.7 $cm^3 \cdot g^{-1}$ for **1**, and 4.7 $cm^3 \cdot g^{-1}$ for **2**) are far below the amounts that should be adsorbed considering the potential void volumes determined from SCXRD data.

Conclusion

This series of preliminary results confirms that with a robust supramolecular synthon such as the ionic H-bonds utilized here, a structure/property tuning becomes possible. This is illustrated by the diamond-type networks formed with the tetrahedral-shaped tetracation which overall supramolecular assemblage was not compromised by the different linear linkers used. As a result, metrics of the resulting adamantanoid cage could be rationally modulated by varying the size of the spacer (from *ca* 2.2 to 6.9 Å) involved in the process.

This investigation aimed also to explore the possibility to form organic open-framework/porous materials by association of cationic H-bond donors and 2-connecting anionic H-bond acceptors. The first results appear promising, four out of the six formed assemblages exhibit open-framework architectures with potential porosities up to 41 %. It can be noticed that these frameworks have been constructed with rather basic molecules as linkers. A continuation of this investigation would be to optimize the chemical design of the H-acceptor to limit the phenomena of net-interpenetration.

Experimental section

Materials and methods:

1,3,5-trisimidazolylbenzene (herein designated as TrIB) and the tetrakis(methoxy-4-pyridyl)methane (Tetrapy) were prepared in good yields according to literature procedures.[18-19] Oxalic acid (H_2Ox), chloranilic acid (H_2CA) and terephtalic acid (H_2BDC) were purchased from commercial sources and used as received.

Physical measurements:

Infrared spectra were recorded with a Perkin-Elmer Spectrum 100 FT-IR spectrometer in the range 4000–600 cm^{-1}. Elemental analyses were performed using a Perkin-Elmer 2400 II, CHNS/O analyzer. TGA measurements have been done on a Perkin-Elmer Diamond TG/DTA Instruments. The compounds were heated at the rate of 1°C/min between RT and 200°C and at the rate of 10°C/min above 200°C/min under N_2 flux. Gas adsorption isotherms

were recorded on evacuated materials on a Micromeritics ASAP 2020 analyzer. Samples were previously degassed at 333 K in vacuo (10^{-5} Torr) for 3 h. CO_2 adsorption experiments were recorded at 25°C using the same instrument.

Crystallographic studies:

X-ray data for compounds **2-5** were collected at low temperature on a GEMINI Oxford-Diffraction diffactometer using Cu radiation (λ = 1.54180 Å), those for compound **1** were collected at 100K on an APEX2 Bruker diffractometer equipped with Mo microfocus source (λ = 0.71073 Å). The structures were solved using SUPERFLIP[26] or SHELXS,[27] and refined by means of least-squares procedures on F using the programs of the PC version of CRYSTALS.[28] Atomic scattering factors were taken from the international tables for X-ray crystallography.[29] Excepted on some solvent molecules, the H atoms were located in a difference map, but those attached to carbon atoms were repositioned geometrically. The H atoms were initially refined with soft restraints on the bond lengths and angles to regularize their geometry and Uiso(H), after which the positions were refined with riding constraints.[30] For **1**, a disorder found for some of the solvent molecules has been refined as half-occupancy DMF molecule (with N47,O45) and the half-occupancy water molecule oxygen O57. Refinement has shown clearly that this is the best model to describe the disorder. For compound **4**, it was not possible to resolve diffuse electron-density residuals (enclosed water solvent molecules). Treatment with the SQUEEZE facility from PLATON resulted in a smooth refinement.[31] The squeeze output implies that 1886 electrons were removed from the unit cell contents, which can be associated to 12 water molecules in the asymmetric unit (Space group I $4_1/a$, general multiplicity = 16) and around 5 water molecules in the overall formulation. The contribution of those disordered water molecules were included in the calculations reported in table 1. CIF for these structures have been deposited at CCDC with references 1402184 to 1402188 respectively for **1** to **5**.

The powder X-ray diffraction patterns were collected in reflexion mode on a XPert Pro (θ–θ mode) Panalytical diffractometer with $\lambda(Cu_{K\alpha1,\ K\alpha2})$ = 1.54059, 1.54439 Å coupled to an Anton Parr oven, or in transmission mode on a Panalytical Empyrean diffractometer using Kapton sheets as a support and the same $Cu_{K\alpha1,\ K\alpha2}$ radiations. All data were collected in 2° < 2θ < 50° range, with 0.02 steps and 10 to 100 s of exposure.

Synthesis:

All compounds were prepared under aerobic conditions using DMF/H_2O mixtures (95/ 5) as solvent. In all cases, same concentrations for TrIB and Tetrapy and identical solvent volumes were used. Yields were determined using formula deduced from Elemental Analyses.

1: H_2CA (38 mg, 0.18 mmol) in 5mL of DMF/H_2O was slowly added to TrIB (33 mg, 0.12 mmol) in 10 mL of the same solvent. The dark violet microcrystalline precipitate which formed immediately was stirred during 5 min before the mixture was heated to 80°C to dissolve the solid. Single crystals of **1** suitable for SCXRD formed upon slow cooling. Yield: 80 % (78 mg, 0.096 mmol). IR (ν, cm^{-1}): 3492, 3411, 3139, 3070, 1652, 1625, 1579, 1540, 1482, 1439, 1374, 1332, 1269, 1198, 1117, 1069, 998, 879, 834, 733, 664, 620. Anal. (%) calcd. for $C_{30.90}H_{37.10}N_{8.30}O_{11.30}Cl_3$: C, 45.71; H, 4.61; N, 14.32; Found: C, 45.48; H, 4.75; N, 14.22.

2: This compound was prepared using the experimental procedure one detailed for **1**, by adding H_2CA (50 mg, 0.24 mmol) in 5mL of DMF/H_2O to Tetrapy (53 mg, 0.12 mmol) in 10 mL of the same solvent. Yield: 72 % (95 mg, 0.086 mmol). IR (ν, cm^{-1}): 3403, 3103, 2920, 2851, 1631, 1591, 1490, 1457, 1316, 1293, 1281, 1192, 1097, 1018, 986, 869, 832, 672, 640. Anal. (%) calcd. for $C_{45.70}H_{51.30}N_{6.90}O_{16.40}$ Cl_4: C, 49.83; H, 4.69; N, 8.77; Found: C, 50.01; H, 4.59; N, 8.63.

3: H_2Ox (17 mg, 0.18 mmol) in 5mL of DMF/H_2O was slowly added to TrIB (33 mg, 0.12 mmol) in 10 mL of the same solvent. After mixing, the reaction mixture was kept undisturbed. Single crystals of **3** suitable for SCXRD were collected after 48h. Yield (after crystallization over 1 week): 38 % (18 mg, 0.034 mmol). IR (ν, cm^{-1}): 3411, 3123, 3103, 3058, 1656, 1615, 1520, 1496, 1289, 1243, 1111, 1073, 1014, 905, 879, 822, 753, 721, 684, 650. Anal. (%) calcd. for $C_{19}H_{25.80}N_6O_{12.90}$: C, 41.90; H, 4.77; N, 15.43; Found: C, 41.72; H, 4.36; N, 15.36.

4: H_2Ox (22 mg, 0.24 mmol) in 5mL of DMF/H_2O was slowly added to Tetrapy (53 mg, 0.12 mmol) in 10 mL of the same solvent. After mixing, the reaction mixture was kept undisturbed. Single crystals of suitable for SCXRD were collected after 24h. Crystallization over 1 week yielded 55 mg (0.078 mmol, Yield = 65 %) of **4**. IR (ν, cm^{-1}): 3363, 3083, 2559, 2917, 1631, 1593, 1502, 1459, 1306, 1283, 1192, 1097, 1012, 964, 836, 765, 664. Anal. (%) calcd. for $C_{29}H_{37.5}N_4O_{16.75}$: C, 49.05; H, 5.32; N, 7.89; Found: C, 49.10; H, 5.41; N, 7.73.

5: H_2BDC (40 mg, 0.24 mmol) in 5mL of DMF/H_2O was slowly added to Tetrapy (53 mg, 0.12 mmol) in 10 mL of the same solvent. After mixing, the reaction mixture was kept undisturbed. Single crystals of **5** suitable for SCXRD were collected after 24h. Yield (after

crystallization over 1 week): 64 % (68 mg, 0.077 mmol). IR (ν, cm^{-1}): 3436, 3103, 2920, 2851, 1660, 1627, 1597, 1506, 1457, 1384, 1277, 1192, 1087, 1014, 850, 731, 624. Anal. (%) calcd. for $C_{44}H_{49}N_5O_{16}$: C: 59.66; H: 5.35; N: 7.91; Found: C: 59.85; H: 5.90; N: 8.04.

Acknowledgments

The authors thank the technical staff of *LCC* for assistance in data acquisition. This work was supported by the Centre National de la Recherche Scientifique (CNRS), by the Région Midi-Pyrénées, under the project "*MOFinMeAl*", and by the Conseil Régional de Bourgogne (programs PARI IME SMT8 and PARI II CDEA). MG and GM are grateful to the University of Toulouse for a scholarship.

References.

1. G. R. Desiraju, *CrystEngComm*, 2003, **5**, 466-467.
2. a) X.-H. Ding, L.-F. Cui, Y.-H. Li, S. Wang and W. Huang, *New J. Chem.*, 2012, **36**, 1884-1890; b) A. Lemmerer, J. Bernsteinz and M. A. Spackman, *Chem. Commun.*, 2012, **48**, 1883-1885.
3. C. B. Aakeroy, N. R. Champness and C. Janiak, *CrystEngComm*, 2010, **12**, 22-43.
4. D. P. McNamara, S. L. Childs, J. Giordano, A. Iarriccio, J. Cassidy, M. S. Shet, R. Mannion, E. O'Donnell and A. Park, *Pharm. Res.*, 2006, **23**, 1888-1897.
5. a) B. K. Saha and S. Bhattacharya, *CrystEngComm*, 2010, **12**, 2369-2373; b) R. Santra, N. Ghosh and K. Biradha, *New J. Chem.*, 2008, **32**, 1673-1676.
6. a) D. Braga, *Chem. Commun.*, 2003, 2751-2754; b) G. R. Desiraju, *Angew. Chem. Int. Ed.*, 1995, **34**, 2311-2327; c) J. C. Macdonald and G. M. Whitesides, *Chem. Rev.*, 1994, **94**, 2383-2420.
7. a) X.-Z. Luo, X.-J. Jia, J.-H. Deng, J.-L. Zhong, H.-J. Liu, K.-J. Wang and D.-C. Zhong, *J. Am. Chem. Soc.*, 2013, **135**, 11684-11687; b) T.-H. Chen, I. Popov, W. Kaveevivitchai, Y.-C. Chuang, Y.-S. Chen, O. Daugulis, A. J. Jacobson and O. S. Miljanic, *Nat. Comm.*, 2014, **5**, 6131; c) P. Li, Y. He, H. D. Arman, R. Krishna, H. Wang, L. Weng and B. Chen, *Chem. Commun.*, 2014, **50**, 13081-13084; d) P. Li, Y. He, J. Guang, L. Weng, J. C.-G. Zhao, S. Xiang and B. Chen, *J. Am. Chem. Soc.*, 2014, **136**, 547-549; e) P. Li, Y. He, Y. Zhao, L. Weng, H. Wang, R. Krishna, H. Wu, W. Zhou, M. O'Keeffe, Y. Han and B. Chen, *Angew. Chem. Int. Ed.*, 2015, **54**, 574-577; f) J. Lue, C. Perez-Krap, M. Suyetin, N. H. Alsmail, Y. Yan, S. Yang, W. Lewis, E. Bichoutskaia, C. C. Tang, A. J. Blake, R. Cao and M. Schroeder, *J. Am. Chem. Soc.*, 2014, **136**, 12828-12831; g) P. Brunet, M. Simard and J. D. Wuest, *J. Am. Chem. Soc.*, 1997, **119**, 2737-2738.
8. a) B. R. Bhogala and A. Nangia, *Cryst. Growth Des.*, 2003, **3**, 547-554; b) B. R. Bhogala, S. K. Chandran, L. S. Reddy, R. Thakuria and A. Nangia, *CrystEngComm*, 2008, **10**, 1735-1738; c) Y.-B. Men, J. Sun, Z.-T. Huang and Q.-Y. Zheng, *CrystEngComm*, 2009, **11**, 978-979; d) Y.-B. Men, J. Sun, Z.-T. Huang and Q.-Y. Zheng, *CrystEngComm*, 2009, **11**, 2277-2278; e) Y.-B. Men, J. Sun, Z.-T. Huang and

Q.-Y. Zheng, *Chem. Commun.*, 2010, **46**, 6299-6301; f) G. K. Kole, G. K. Tan, L. L. Koh and J. J. Vittal, *CrystEngComm*, 2012, **14**, 6190-6195.
9. S. J. Dalgarno, P. K. Thallapally, L. J. Barbour and J. L. Atwood, *Chem. Soc. Rev.*, 2007, **36**, 236-245.
10. V. A. Blatov, L. Carlucci, G. Ciani and D. M. Proserpio, *CrystEngComm*, 2004, **6**, 377-395.
11. T. R. Shattock, K. K. Arora, P. Vishweshwar and M. J. Zaworotko, *Cryst. Growth Des.*, 2008, **8**, 4533-4545.
12. a) T. Leyssens, G. Springuel, R. Montis, N. Candoni and S. Veesler, *Cryst. Growth Des.*, 2012, **12**, 1520-1530; b) D. Braga, S. L. Giaffreda, K. Rubini, F. Grepioni, M. R. Chierotti and R. Gobetto, *CrystEngComm*, 2007, **9**, 39-45.
13. a) M. Meot-Ner, *Chem. Rev.*, 2012, **112**, PR22; b) M. D. Ward, *Chem. Commun.*, 2005, 5838-5842.
14. a) V. A. Russell, C. C. Evans, W. J. Li and M. D. Ward, *Science*, 1997, **276**, 575-579; b) K. T. Holman, A. M. Pivovar, J. A. Swift and M. D. Ward, *Acc. Chem. Res.*, 2001, **34**, 107-118; c) K. T. Holman, A. M. Pivovar and M. D. Ward, *Science*, 2001, **294**, 1907-1911.
15. a) A. Yamamoto, S. Uehara, T. Hamada, M. Miyata, I. Hisaki and N. Tohnai, *Cryst. Growth Des.*, 2012, **12**, 4600-4606; b) A. Yamamoto, T. Hamada, I. Hisaki, M. Miyata and N. Tohnai, *Angew. Chem. Int. Ed.*, 2013, **52**, 1709-1712.
16. A. Yamamoto, T. Hasegawa, T. Hamada, T. Hirukawa, I. Hisaki, M. Miyata and N. Tohnai, *Chem. Eur. J.*, 2013, **19**, 3006-3016.
17. a) G. Mouchaham, N. Roques, I. Imaz, C. Duhayon and J.-P. Sutter, *Cryst. Growth Des.*, 2010, **10**, 4906-4919; b) G. Mouchaham, N. Roques, A. Kaiba, P. Guionneau and J.-P. Sutter, *CrystEngComm*, 2010, **12**, 3496-3498; c) G. Mouchaham, N. Roques, S. Brandes, C. Duhayon and J.-P. Sutter, *Cryst. Growth Des.*, 2011, **11**, 5424-5433; d) G. Mouchaham, N. Roques, C. Duhayon, I. Imaz and J.-P. Sutter, *New J. Chem.*, 2013, **37**, 3476-3487; e) N. Roques, G. Mouchaham, C. Duhayon, S. Brandes, A. Tachon, G. Weber, J. P. Bellat and J.-P. Sutter, *Chem. Eur. J.*, 2014, **20**, 11690-11694; f) F. Thétiot, C. Duhayon, T. S. Venkatakrishnan and J.-P. Sutter, *Cryst. Growth Des.*, 2008, **8**, 1870-1877.
18. J. Fan, L. Gan, H. Kawaguchi, W. Y. Sun, K. B. Yu and W. X. Tang, *Chem. Eur. J.*, 2003, **9**, 3965-3973.
19. P. E. Ryan, C. Lescop, D. Laliberte, T. Hamilton, T. Maris and J. D. Wuest, *Inorg. Chem.*, 2009, **48**, 2793-2807.
20. E. Krogh Andersen, *Acta Cryst.*, 1967, **22**, 196-201.
21. *Note*: Additional solvent molecules have been detected but these were highly disordered and were not refined. The residual electronic density suggested ca. 0.25 DMF and 0.5 H2O, which is confirmed by chemical analysis.
22. N. Roques, D. Maspoch, A. Datcu, K. Wurst, D. Ruiz-Molina, C. Rovira and J. Veciana, *Polyhedron*, 2007, **26**, 1934-1948.
23. S. R. Batten, N. R. Champness, X.-M. Chen, J. Garcia-Martinez, S. Kitagawa, L. Ohrstrom, M. O'Keeffe, M. P. Suh and J. Reedijk, *CrystEngComm*, 2012, **14**, 3001-3004.
24. A. L. Spek, *PLATON, A Multipurpose Crystallographic Tool*, Utrecht (The Netherlands), Utrech University, 2001.
25. *Note*: Fits have been performed with Le Bail algorythm implemented in Highscore+ package supplied by Panalytical.
26. L. Palatinus and G. Chapuis, *J. Appl. Cryst.*, 2007, **40**, 786-790.
27. G. M. Sheldrick, *Acta Cryst. A*, 2008, **64**, 112-122.

28. P. W. Betteridge, J. R. Carruthers, R. I. Cooper, K. Prout and D. J. Watkin, *J. Appl. Cryst.*, 2003, **36**, 1487.
29. *International Tables for X-ray Crystallography*, Kynoch Press, Birmingham, England, 1974.
30. R. I. Cooper, A. L. Thompson and D. J. Watkin, *J. Appl. Cryst.*, 2010, **43**, 1100-1107.
31. P. v. d. Sluis and A. L. Spek, *Acta Cryst.*, 1990, **A46**, 194-201.